Supplemental Information

Supplemental Methods

MRI Data Preprocessing

IU Dataset. We conducted one additional preprocessing pipeline: slice-time-corrected conventional GLM preprocessing. This preprocessing method was identical to conventional GLM preprocessing (described in *Methods*), with one additional step: slice time correction was performed immediately following motion correction and fieldmap unwarping.

HCP Dataset. We conducted one additional preprocessing pipeline – respiratory preprocessing – upon the subset of 130 HCP scans for which we had all four runs available and complete physiological recordings. Using FSL PNM we generated 9 slice-time corrected versions of the same respiratory regressors described in the main Methods (8 RETROICOR-style regressors and RVT). We added one additional respiratory regressor, convolving the RVT trace with the respiratory response function (RRF) defined by Birn and colleagues (2008), for each slice-time-corrected version of the RVT trace. Then beginning with the "minimally preprocessed" nifti files, we conducted a voxel-level respiratory cleanup. We note at the outset that one limitation of this cleanup is that although it is preferable to remove respiratory-stage variance in native space at an early stage of preprocessing, the earliest stage data we had available was minimally preprocessed (as described in Glasser et al., 2013) and already registered to standard space. For each voxel, we followed a four-step process in order to remove the best estimate of respiratory variance while retaining the

most degrees of freedom in the data (as recommended by Bright, Tench, and Murphy, 2017). First, for each of the 10 respiratory regressors, we selected the slice-time-corrected variant of that regressor that was most correlated (positively or negatively) with that voxel's time series. Next, for each of those 10 selected respiratory regressors, we created time-shifted versions from 1 to 12 TRs forward and backward in time. Then, again for each of the 10 regressors, we selected the time-shifted variant that was most correlated (positively or negatively) with the voxel time series (see also Birn et al., 2006; 2008; Tong et al., 2011; Bright et al., 2017). This resulted in a total of 10 best-fitting respiratory regressors (one of each type, 8 RETROICOR-style, RVT, and RVT convolved with RRF) that were then regressed from the voxel time series. This process was repeated at each voxel and the resulting residuals were analyzed as the "respiratory preprocessing".

Analysis

Assessment of lagged residual structure outside the cortex. We also examined lagged residual BOLD structure in the white matter and CSF compartments, by repeating the main analysis using the mean signal within each compartment. We also repeated the main grayordinates analysis (Fig. 5) using volumetric nifti data, with the only difference being the examination of voxel time series in the white matter and in the CSF. As before, to limit computational demands, the voxel-level analysis was restricted to the subset of 40 HCP subjects where all 4 runs were available.

Relationships between respiratory response function (RRF) and residual lagged structure associated with FD and RVT traces. Given our conjecture that the lagged FD-linked residual structure observed in Fig. 1 is related to lagged effects of respiration changes, we examined the similarity between the respiration response function (RRF; Birn et al., 2008), which explicitly models lagged effects of changes in depth and rate of respiration, and the residual structure we observed to be associated with FD and with RVT. We computed the absolute values of correlations between the RRF and the first 28 seconds (the duration of the RRF) of residual structure associated with each FD range (or RVT range). To assess the possibility of a temporal offset between patterns, we also examined correlations between the residual structure and time-shifted versions of the RRF from 1 to 6 TRs forward and backward in time.

Supplemental Figures

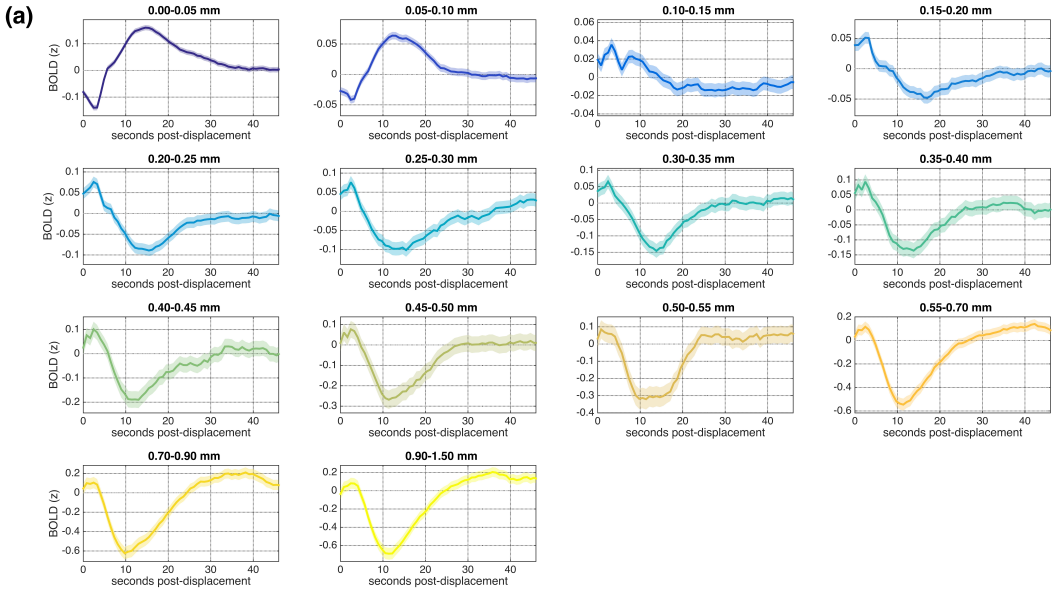

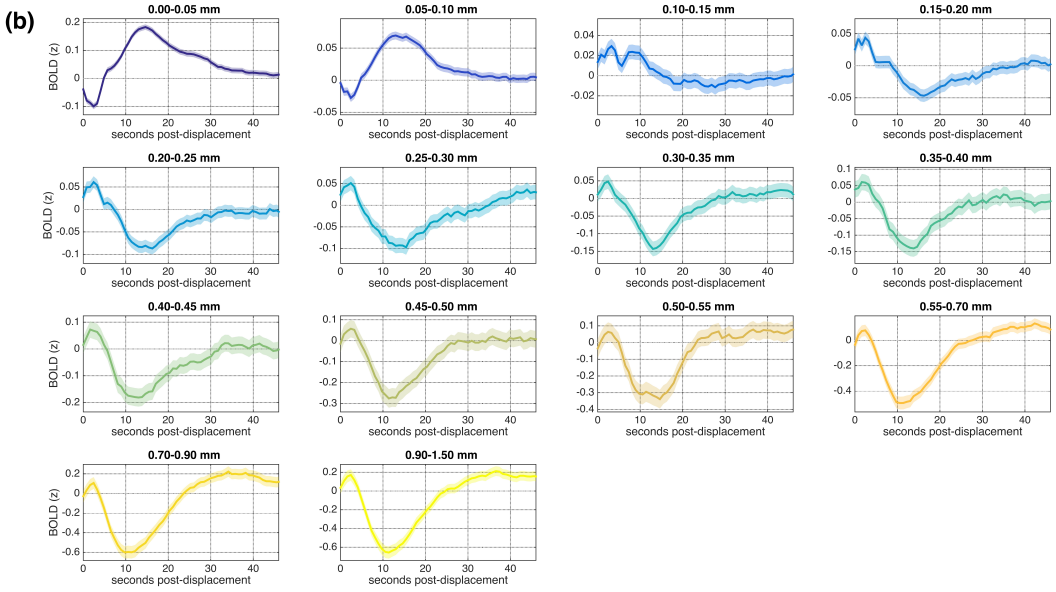

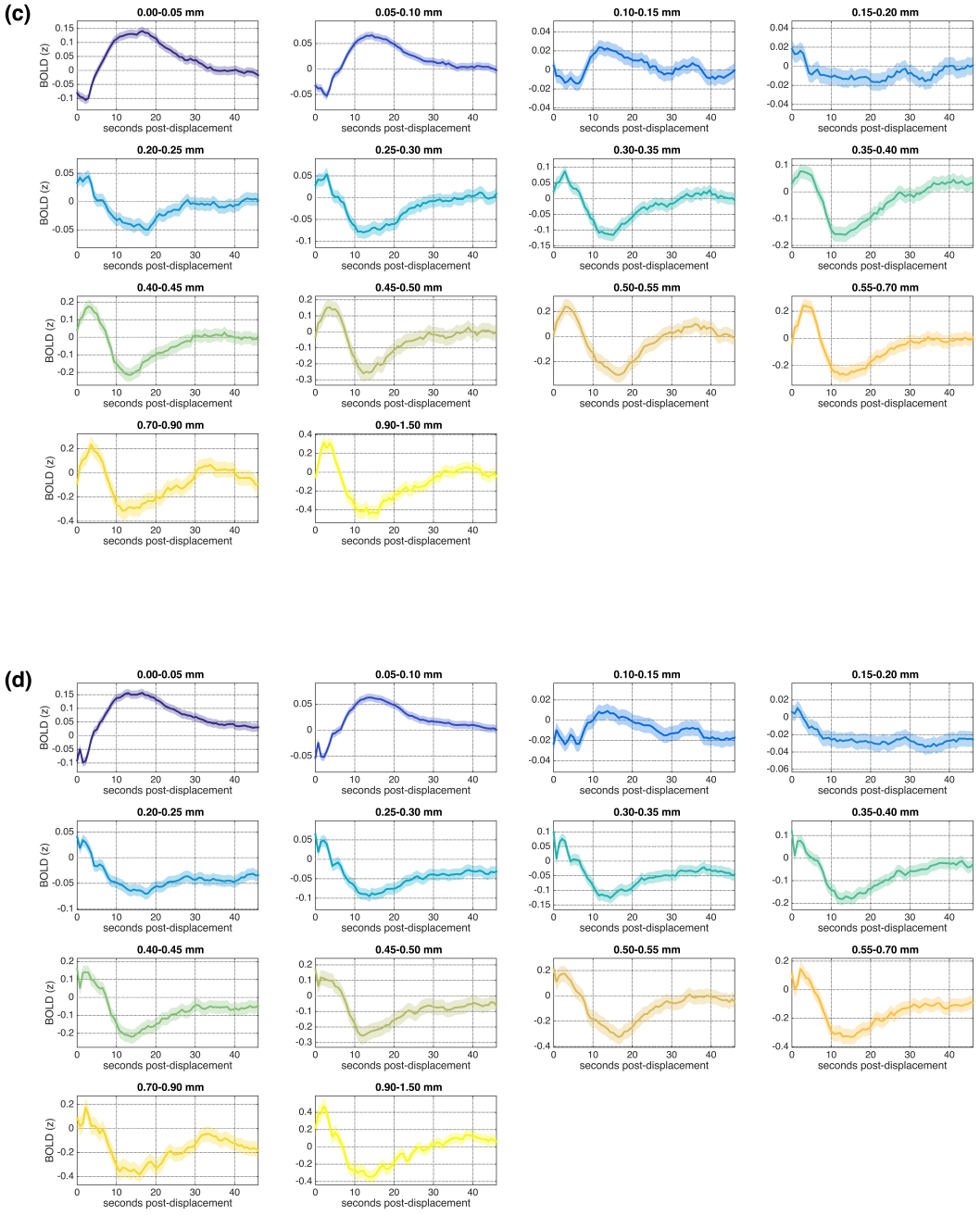

Supplemental Figure 1. Mean cortical BOLD signal following framewise displacements of similar magnitudes along with 95% confidence intervals, presented not for inference but for closer examination of the patterns and range of variability. (a) IU dataset; FIX preprocessing.

(b) HCP dataset; FIX preprocessing. (c) IU dataset; GLM preprocessing. (d) HCP dataset; minimal preprocessing.

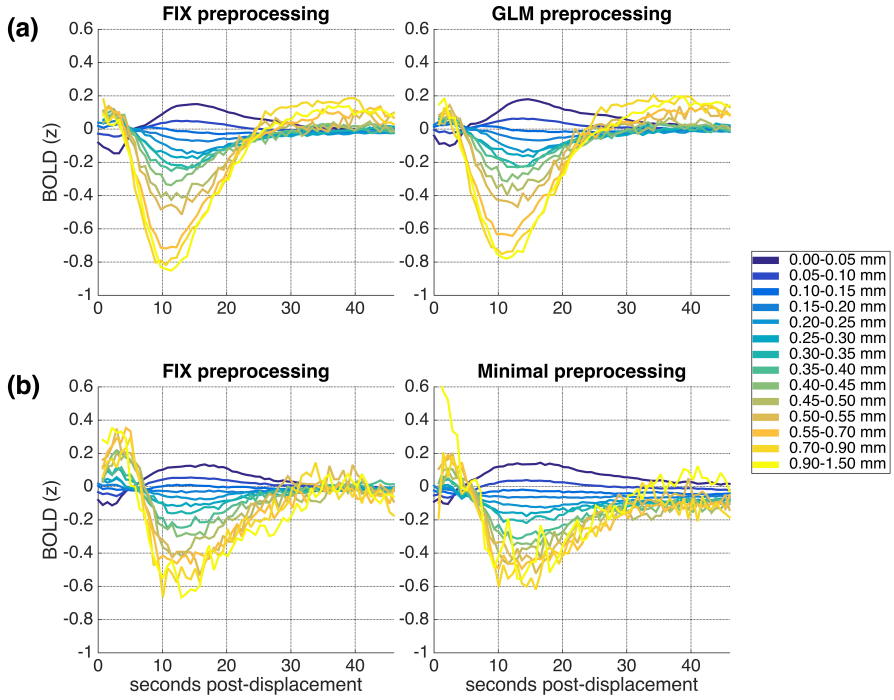

Supplemental Figure 2. Mean cortical BOLD signal following framewise displacements of similar magnitudes, after censoring all TRs with FD >= 0.2mm. (a) IU dataset, FIX (left) and GLM (right) preprocessing. (b) HCP dataset, FIX (left) and Minimal (right) preprocessing.

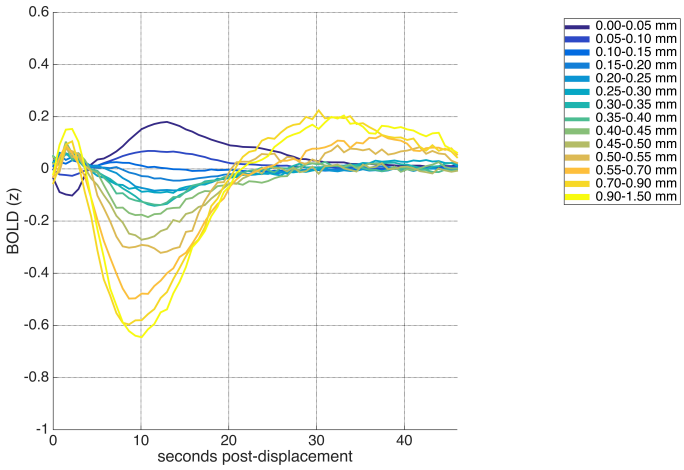

Supplemental Figure 3. Mean cortical BOLD signal following framewise displacements of similar magnitudes, IU dataset with slice timing correction followed by GLM preprocessing.

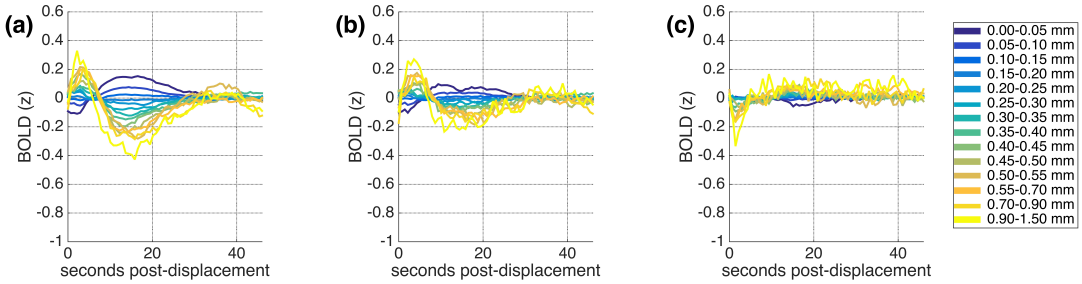

Supplemental Figure 4. Mean BOLD signal following framewise displacements of similar magnitudes, for HCP FIX dataset, across (a) cortical voxels, (b) white matter voxels, and (c) CSF voxels.

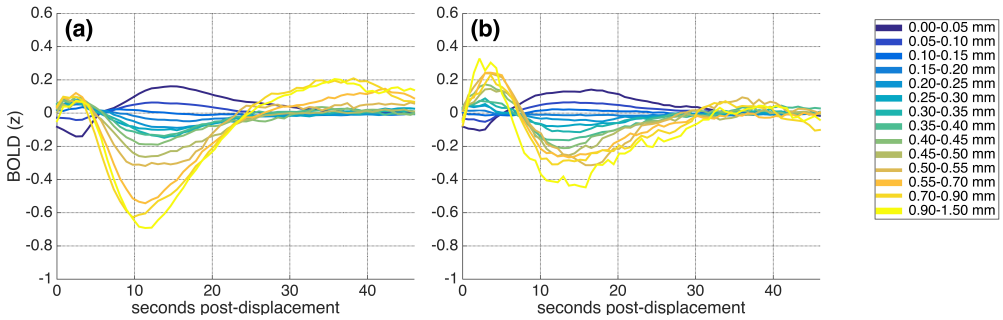

Supplemental Figure 5. Mean patterns across all 20 iterations of downsampled analysis (Check 2), in which the main analysis is performed using only non-overlapping BOLD epochs separated by 20 TRs. (a) IU and (b) HCP datasets with FIX preprocessing. Patterns are effectively the same as depicted in Figure 1.

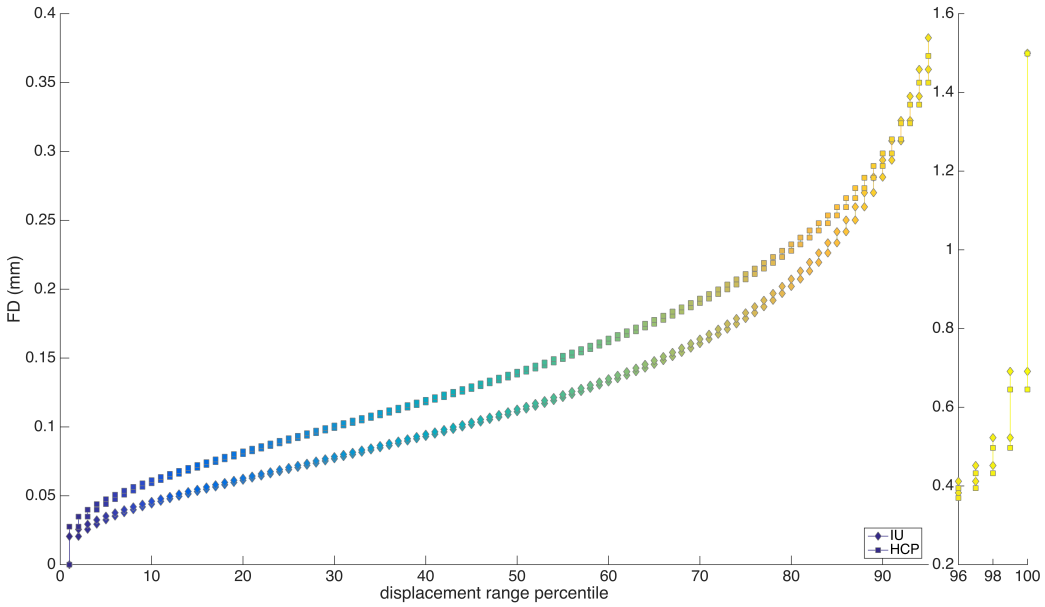

Supplemental Figure 6. Minimum and maximum of 100 percentile-based displacement ranges for IU (diamonds) and HCP (squares) datasets. Percentiles 96-100 are plotted separately to facilitate inspection of the data.

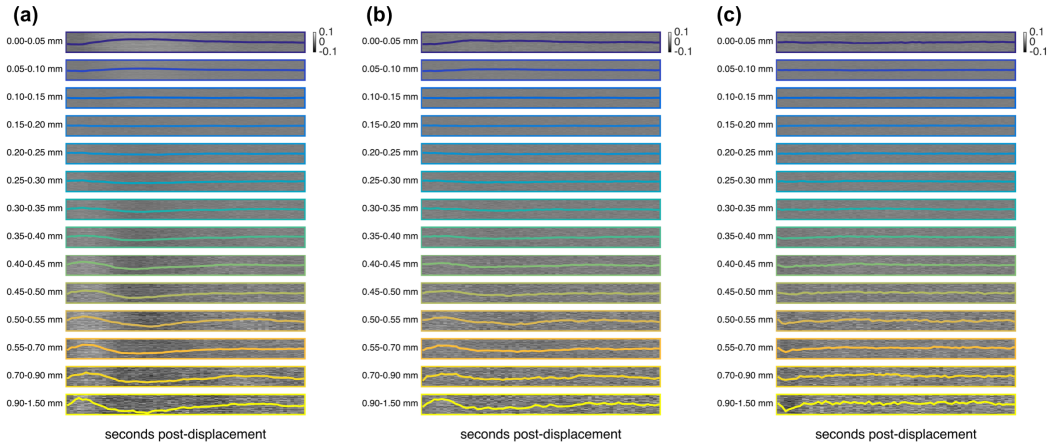

Supplemental Figure 7. Main analysis performed at individual voxels for HCP data with FIX preprocessing. Rows of the rasters correspond to voxels, with each row depicting the mean BOLD signal following similar framewise displacements at that voxels, from 0 to 46 seconds post-displacement, for each compartment (a, gray matter voxels; b, white matter voxels; c, CSF voxels). We plot the same randomly selected 20% of all voxels in each compartment in each of the 14 rasters. Grayscale color axis is the same for all 42 rasters. The mean BOLD signal for each displacement range from that compartment (previously presented in Supp. Fig. 4 above) is superimposed in color (note that scales for the mean BOLD signal only are not comparable across a-c, so that the patterns within each compartment can be most clearly visualized). Figure 7a is effectively identical to Fig. 5, and is presented here for ease of comparison.

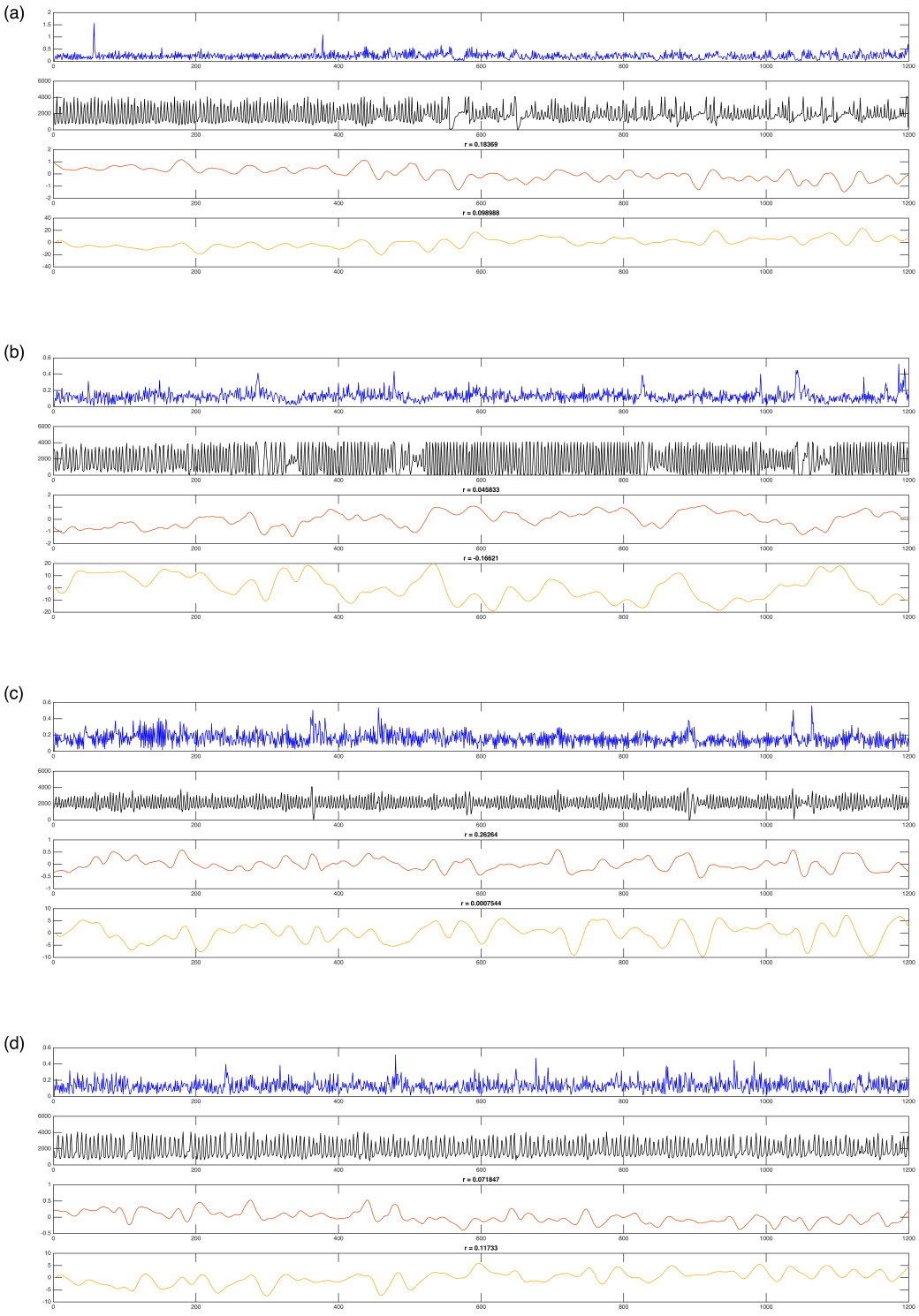

Supplemental Figure 8. Nuisance traces for the same example subjects and scans in Figure 6b, presented in the same order. Each figure plots, from top to bottom, framewise displacement

(blue), raw respiratory recording (sampled at the TR trigger; black), RVT (red), and RVT convolved with RRF (yellow). Correlations are between framewise displacement and the plotted respiratory regressor. See also Supplemental Table 3 for summary statistics across all subjects.

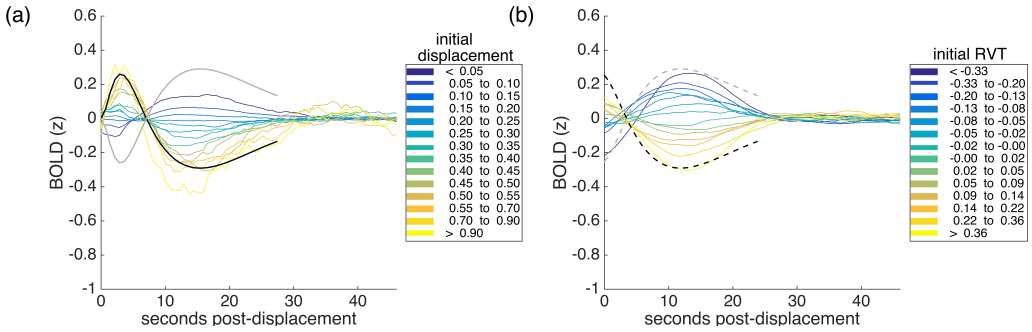

Supplemental Figure 9. Relationships between the respiratory response function (RRF) and the residual lagged structure associated with FD and RVT, using HCP data with FIX preprocessing. Correspondence between the RRF and lagged residual structure (defined as the mean of the absolute value of the correlations between the RRF and the residual pattern for each of the 14 ranges) was greatest between the FD-linked residual structure with no time-shifting (mean (SD) of abs(r) = .92 (.05)); correspondence was greatest with the RVT-linked residual structure when the RRF was shifted backward by 5 TRs (mean (SD) of abs(r) = .93 (.05)). (a) FD-linked residual structure (see also Fig. 1b, left) with RRF overlaid (+RRF, black; -RRF, gray) with no time-shifting. (b) RVT-linked residual structure (see also Fig. 11a) with RRF shifted backward by 5 TRs overlaid (+RRF, black dotted line; -RRF, gray dotted line). Note that in both (a) and (b) the RRF was scaled by 0.3 in order to fit on the same axes as the residual lagged structure.

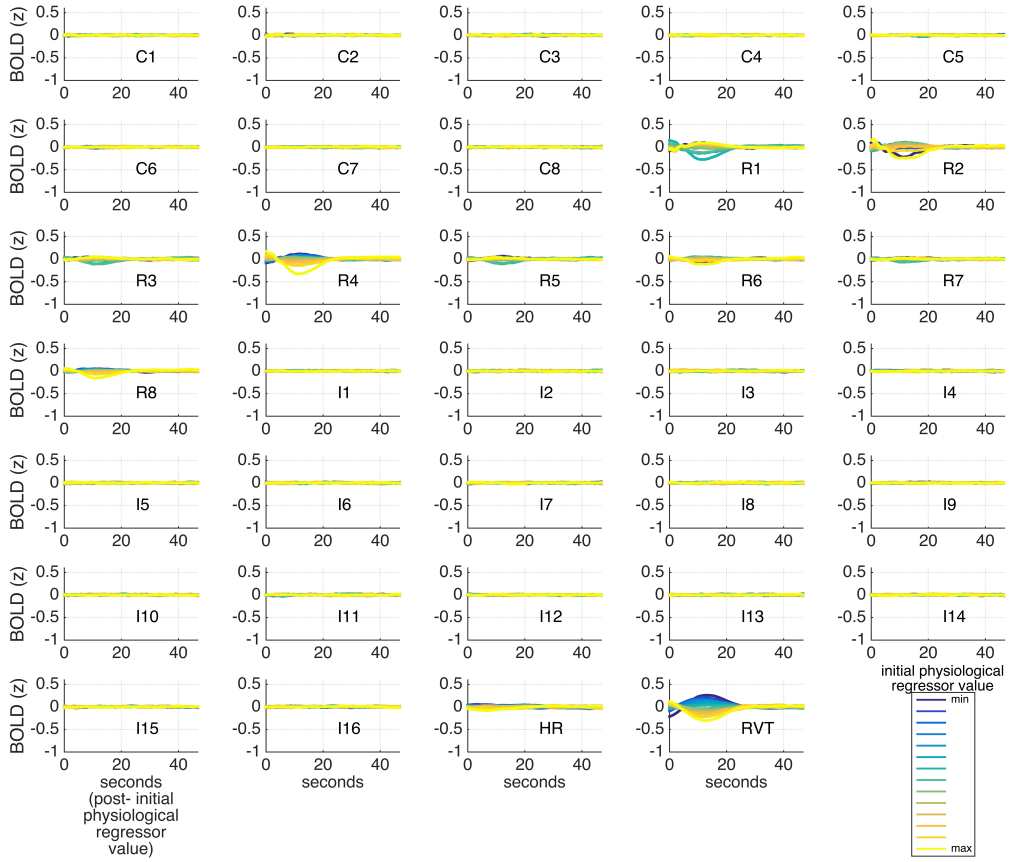

Supplemental Figure 10. Mean cortical BOLD signal following initial physiological regressor values of similar magnitudes, for HCP dataset with FIX preprocessing, for all 34 physiological regressors examined. RETROICOR-style regressors are labeled C for cardiac, R for respiratory, and I for interactions between cardiac and respiratory phases. Regressors C1-8 and R1-8 refer to sin(p), cos(p), sin(2p), cos(2p), sin(3p), cos(3p), sin(4p), and cos(4p), where p *is the cardiac phase* c *or respiratory phase* r*. Regressors I1-16 refer to cos(c+r), sin(c+r), cos(c-r), sin(c-r), cos(c+2r), sin(c+2r), cos(c-2r), sin(c-2r), cos(2c+r), sin(2c+r), cos(2c-r), sin(2c-r), cos(2c+2r), sin(2c+2r), cos(2c-2r), sin(2c-2r). HR refers to heartrate and RVT refers to respiration volume per time (Birn et al., 2006).*

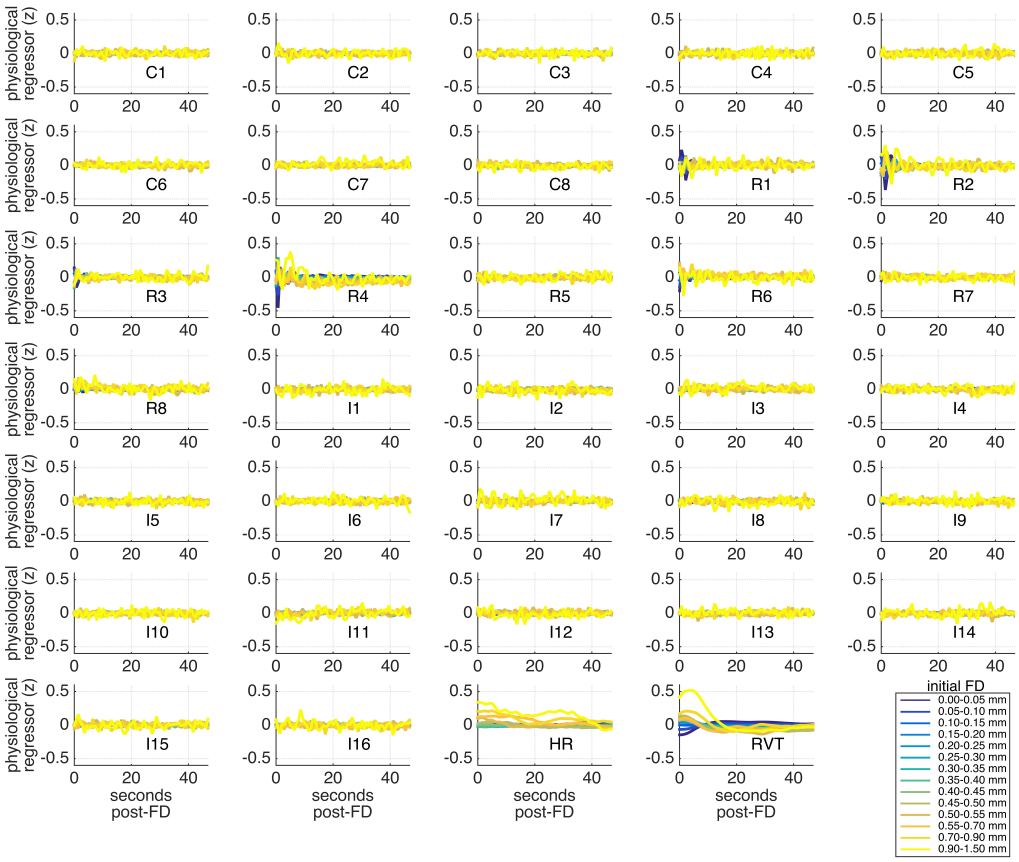

Supplemental Figure 11. Mean physiological regressor epochs following framewise displacements of similar magnitudes, for HCP dataset with FIX preprocessing, for all 32 physiological regressors examined. Each physiological regressor is z-scored before combining across runs and averaging. See Supplemental Figure 10 for key to regressor labels.

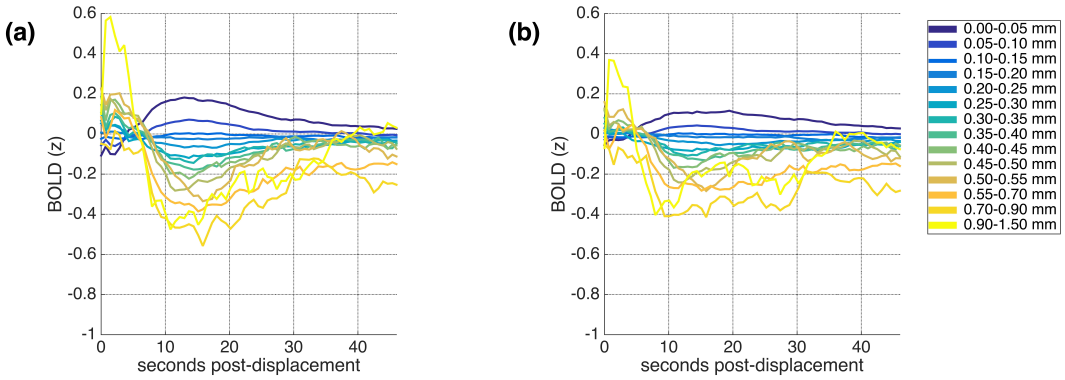

Supplemental Figure 12. Mean cortical BOLD signal following framewise displacements of similar magnitudes, for a subset of 130 scans from the HCP dataset that had physiological recordings available. (a) Minimal preprocessing only; (b) Minimal preprocessing with voxel-level respiratory cleanup.

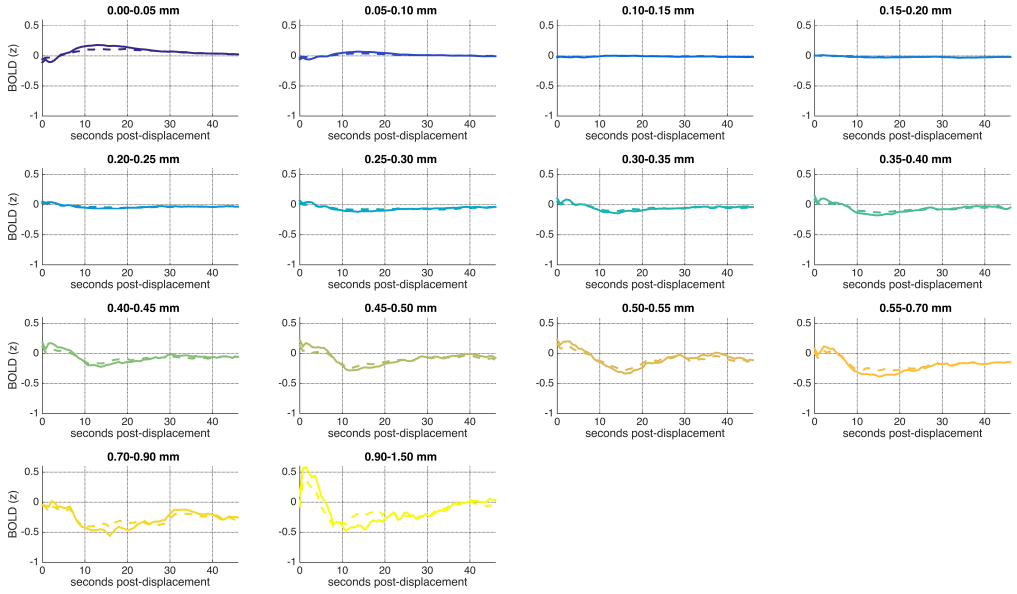

Supplemental Figure 13. Mean cortical BOLD signal following framewise displacements of similar magnitudes, for a subset of 130 scans from the HCP dataset that had physiological

recordings available. Plots depict the mean cortical BOLD signal for each displacement range following minimal preprocessing only (solid line) and minimal preprocessing with voxel-level respiratory cleanup (dashed line), for comparison purposes.

Supplemental Tables

Displacement Range	IU dataset (%)	HCP dataset (%)
0-.05 mm	12.35	5.84
.05-.1 mm	30.91	24.05
.1-.15 mm	22.54	25.1
.15-.2 mm	12.92	17.88
.2-.25 mm	7.24	11.39
.25-.3 mm	4.37	6.74
.3-.35 mm	2.99	3.81
.35-.4 mm	2.08	2.11
.4-.45 mm	1.31	1.09
.45-.5 mm	0.8	0.63
.5-.55 mm	0.47	0.39
.55-.7 mm	0.76	0.56
.7-.9 mm	0.48	0.25
.9-1.5 mm	0.47	0.14
>1.5mm (excluded)	*0.031*	*0.003*

Supplemental Table 1. Percentage of all FD instances within each displacement range in IU and HCP datasets.

Displacement Range	IU dataset			HCP dataset		
	# FC Matrices	# Unique Subjects	# FC Matrices / Subject	# FC Matrices	# Unique Subjects	# FC Matrices / Subject
0-.05 mm	35504.79 (543.97)	51	696.17 (575.98)	13948.15 (196.76)	71	196.45 (191.12)
.05-.1 mm	85991.86 (1355.45)	51	1686.11 (916.74)	56916.62 (934.43)	72	790.51 (506.08)
.1-.15 mm	60007.74 (963.72)	51	1176.62 (556.67)	57443.47 (909.81)	72	797.83 (422.97)
.15-.2 mm	32056.95 (568.19)	51	628.57 (356.78)	39421.42 (658.67)	72	547.52 (286.49)
.2-.25 mm	15490.58 (300.33)	51	303.74 (205.39)	23280.23 (396.32)	72	323.34 (199.41)
.25-.3 mm	7276.86 (131.71)	51	142.68 (107.01)	11989.50 (217.03)	72	166.52 (120.21)
.3-.35 mm	3607.21 (68.37)	51	70.73 (57.39)	5588.36 (99.31)	72	77.62 (63.20)
.35-.4 mm	1980.70 (38.46)	51	38.84 (34.18)	2494.05 (49.79)	71	35.13 (29.71)
.4-.45 mm	1107.83 (24.81)	49	22.61 (21.18)	1051.35 (19.83)	68	15.46 (14.54)
.45-.5 mm	771.05 (13.36)	48	16.06 (16.90)	510.55 (11.05)	64	7.98 (8.16)
.5-.55 mm	533.30 (10.38)	45	11.85 (12.59)	318.12 (5.87)	58	5.50 (4.66)
.55-.7 mm	1026.89 (20.87)	45	22.82 (25.32)	415.80 (7.95)	58	7.17 (6.43)
.7-.9 mm	701.94 (15.08)	37	18.97 (23.08)	195.35 (1.32)	44	4.45 (3.53)
.9-1.5 mm	795.65 (19.85)	34	23.40 (29.34)	134.24 (2.31)	35	3.88 (4.75)

Supplemental Table 2. Sample sizes for FC analysis, after excluding windows that are more than 50% censored at FD >= 0.2mm. # FC matrices: mean (SD) of the total number of FC matrices included, across all sliding windows for a given displacement range, across all scans. # Unique subjects: number of unique individuals that contributed FC matrices for a given displacement range. # FC matrices per subject: mean (SD) of the number of matrices contributed by each contributing subject for that displacement range, across all sliding windows.

	Correlation between FD & regressor [mean (SD) across scans]	Correlation between standard deviation of FD & of regressor across scans [*r* (*p*)]
R1	-0.031 (0.12)	0.038 (.61)
R2	-0.093 (0.12)	0.078 (.3)
R3	-0.1 (0.21)	0.16 (.04)
R4	-.08 (0.26)	-0.13 (.077)
R5	0.019 (0.086)	0.019 (.8)
R6	0.13 (0.11)	.011 (.88)
R7	-0.014 (0.07)	-0.09 (.19)
R8	0.015 (0.093)	0.097 (.19)
RVT	0.064 (0.13)	0.0057 (.94)
RVT conv. w/RRF	0.035 (0.083)	-0.0013 (.99)

Supplemental Table 3. Relationships between framewise displacement and respiratory traces. Column 1: Mean (SD) across scans of the correlations between framewise displacement traces and each respiratory regressor. Column 2: r (p) for correlation across scans between the standard deviation of the framewise displacement trace and the standard deviation of each respiratory regressor. See Supplemental Figure 10 for key to regressor labels.

Supplemental References

Bright, M. G., Tench, C. R., & Murphy, K. (2017). Potential pitfalls when denoising resting state fMRI data using nuisance regression. *NeuroImage*, *154*, 159-168.

Tong, Y., Hocke, L. M., & Frederick, B. B. (2011). Isolating the sources of widespread physiological fluctuations in functional near-infrared spectroscopy signals. *Journal of biomedical optics*, *16*(10), 106005-106005.